Cytotoxicity and Genotoxicity of Silver Nanoparticles in Human Cells

P. V. AshaRani,[†,‡] Grace Low Kah Mun,[‡] Manoor Prakash Hande,[‡] and Suresh Valiyaveettil[†,*]

[†]Department of Chemistry, Faculty of Science, 3 Science Drive 3, National University of Singapore, Singapore 117543, and [‡]Department of Physiology, Yong Loo Lin School of Medicine, 2 Medical Drive, National University of Singapore, Singapore 117597

ABSTRACT Silver nanoparticles (Ag-np) are being used increasingly in wound dressings, catheters, and various household products due to their antimicrobial activity. The toxicity of starch-coated silver nanoparticles was studied using normal human lung fibroblast cells (IMR-90) and human glioblastoma cells (U251). The toxicity was evaluated using changes in cell morphology, cell viability, metabolic activity, and oxidative stress. Ag-np reduced ATP content of the cell caused damage to mitochondria and increased production of reactive oxygen species (ROS) in a dose-dependent manner. DNA damage, as measured by single cell gel electrophoresis (SCGE) and cytokinesis blocked micronucleus assay (CBMN), was also dose-dependent and more prominent in the cancer cells. The nanoparticle treatment caused cell cycle arrest in G_2/M phase possibly due to repair of damaged DNA. Annexin-V propidium iodide (PI) staining showed no massive apoptosis or necrosis. The transmission electron microscopic (TEM) analysis indicated the presence of Ag-np inside the mitochondria and nucleus, implicating their direct involvement in the mitochondrial toxicity and DNA damage. A possible mechanism of toxicity is proposed which involves disruption of the mitochondrial respiratory chain by Ag-np leading to production of ROS and interruption of ATP synthesis, which in turn cause DNA damage. It is anticipated that DNA damage is augmented by deposition, followed by interactions of Ag-np to the DNA leading to cell cycle arrest in the G_2/M phase. The higher sensitivity of U251 cells and their arrest in G_2/M phase could be explored further for evaluating the potential use of Ag-np in cancer therapy.

KEYWORDS: silver nanoparticle · cytotoxicity · genotoxicity · DNA damage · micronucleus · cell cycle arrest

Nanoparticles are used in bioapplications such as therapeutics,[1] antimicrobial agents,[2] transfection vectors,[3] and fluorescent labels.[4] Despite the rapid progress and early acceptance of nanobiotechnology, the potential for adverse health effects due to prolonged exposure at various concentration levels in humans and the environment has not yet been established. However, the environmental impact of nanomaterials is expected to increase substantially in the future. In particular, the behavior of nanoparticles inside the cells is still an enigma, and no metabolic and immunological responses induced by these particles are understood so far. Nanotoxicology takes up this challenge to decipher the molecular events that regulate bioaccumulation and toxicity of nanoparticles. Silver nanoparticles (Ag-np) have gained much popularity recently owing to the broad spectrum of antimicrobial activity.[5−7] Silver impregnated catheters[8] and wound dressings[9] are used in therapeutic applications. In spite of the wide usage of Ag-np in wound dressings, which can cause easy entry into the cells, very few reports on the toxicity of silver nanoparticles are available. Our study aims to unravel the cellular events that occur upon exposure to silver nanoparticles. Moreover, the mechanisms involved in the toxicity of nanoparticles to microorganisms can also be active in humans. The larger surface area and smaller size of the nanoparticles are expected to increase the *in vivo* activity. Although a few research groups have investigated the toxicity of silver nanocomposites and nanoparticles in cell lines to estimate viability and reactive oxygen species (ROS) generation,[10−13] little is known about the mechanisms of silver nanoparticle toxicity. Recent reports have established involvement of mitochondria-dependent jun-N terminal kinase (JNK) pathway in Ag-np toxicity.[14] *In vivo* experiments in rats have established lung function changes and inflammation.[15] We had reported that silver nanoparticles stabilized with starch and BSA induce distinct developmental defects in zebrafish embryos.[16] However, the primary targets of Ag-np and distribution patterns remain unexplored. Here, an effort to understand various steps in silver nanoparticle toxicity by studying the effect of starch-coated Ag-np on cell viability, ATP production, DNA damage, chromosomal aberrations, and cell cycle is established.

*Address correspondence to chmsv@nus.edu.sg.

Received for review July 2, 2008 and accepted December 16, 2008.

Published online December 30, 2008.
10.1021/nn800596w CCC: $40.75

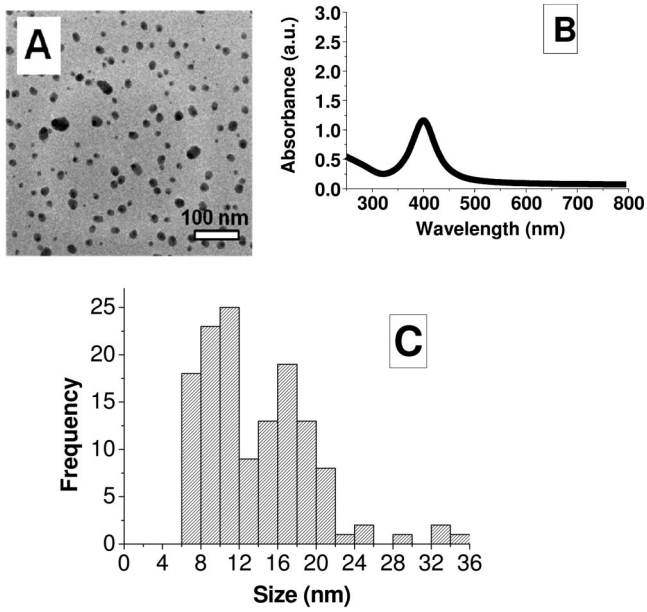

Figure 1. Typical TEM image (A) and UV−visible spectrum (B) of Ag-starch nanoparticles reconstituted after lyophilization. Absorbance maximum at 400 nm and narrow peak indicate small size of the particles. The size distribution histogram generated using image (A) captured with JEOL JSM 2010F showed nanoparticles of size between 6 and 20 nm (C). Analyses were performed from the stock solution reconstituted after lyophilization.

RESULTS AND DISCUSSION

It is expected that the biokinetics of nanoparticles, which is measured as the rate of nanoparticle uptake, intracellular distribution, and exocytosis, contribute tremendously to their toxicity. The nanoparticle size, surface area, and surface functionalization are major factors that influence biokinetics and thus toxicity.[17,18] The nanoparticles employed in this study were of 6−20 nm in size (Figure 1A) with an absorption maximum at 400 nm (Figure 1B). The calculated size distribution histogram confirmed the size distribution of nanoparticles (Figure 1C). These nanoparticles showed good stability in water.[19] Our experiments unveiled a concentration-dependent cytotoxicity (low metabolic activity), genotoxicity (DNA damage and chromosomal aberrations), and cell cycle arrest in Ag-np treated cells. The electron micrographs showed presence of endosomes with nanoparticles in the cytosol, suggesting receptor-mediated endocytosis.

Effect on Cell Morphology. The first and most readily noticeable effect following exposure of cells to toxic materials is the alteration in cell shape or morphology in a monolayer culture. Microscopic observations of treated cells showed distinct morphological changes indicating unhealthy cells, whereas the control appeared normal (Figure 2A). Nanoparticle treated cells appeared to be clustered with a few cellular extensions, and cell spreading patterns were restricted as compared to control cells. This could be due to disturbances in cytoskeletal functions as a consequence of nanoparticle treatment. Similar results were observed by other groups in

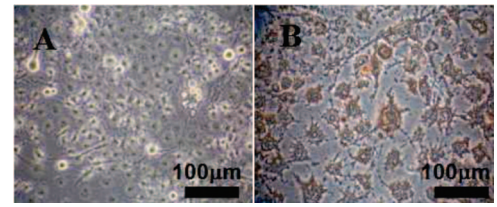

Figure 2. Optical micrographs of U251 cells without any nanoparticle treatment (A) and cells treated with Ag-starch (200 μg/mL) (B). Dark orange patches are visible on the cell surface of the treated cells and remained even after repeated washings.

dermal fibroblast cells treated with citrate-coated gold nanoparticles.[20] Dark orange patches seen on the cell surface may be due to the adsorption of nanoparticles on the cell surface (Figure 2B). However, only a few floating cells were observed under the microscope, suggesting the absence of widespread cell death due to necrosis.

Cell Viability. Viability assays are vital steps in toxicology that explain the cellular response to a toxicant. Also, they give information on cell death, survival, and metabolic activities. We have exploited the high sensitivity of luminescence-based assay and fluorescent-based assay to study the activity of Ag-np. ATP assays to assess the toxicity of silver nanoparticles (Figure 3A) showed a concentration- and time-dependent drop in luminescence intensity in cancer cells and normal cells, signifying time- and dose-dependent toxicity. The ATP content of the cells was not significantly affected at 24 h of incubation in the presence of nanoparticles. ATP content dropped drastically after 48 h, and the same trend was seen up to 72 h. It is noteworthy that the adverse effects of nanoparticles were also concentration-dependent. In the case of nanoparticle agglomeration and subsequent precipitation, uptake rate of nanoparticles will drop, which could be observed as a decrease in ATP depletion and cytotoxicity. When starch alone was used as control, it showed no significant cytotoxicity in both cells (Figure 3B). This observation ensures biocompatibility of starch as capping agent in nanoparticles. Another challenge in nanoparticle toxicity studies was the purity of nanoparticles employed for the study. The nanoparticles should be free from reactants used in the synthetic steps. To check the presence of any toxic materials left over from the synthesis, toxicity studies were done using the supernatant liquid obtained after centrifugation of nanoparticle solution, which is expected to contain excess of reagents, if any. Our results showed no evidence of toxicity for this supernatant liquid. The cell viability in all the wells was comparable to that of control (Figure 3C).

Microscopic observation of treated cells showed no indication of massive cell death. Absence of large number of floating cells even after prolonged incubation period together with a low ATP levels implies a potential for metabolic arrest. Hence metabolic activity studies were conducted using MTS assay and cell titer blue as-

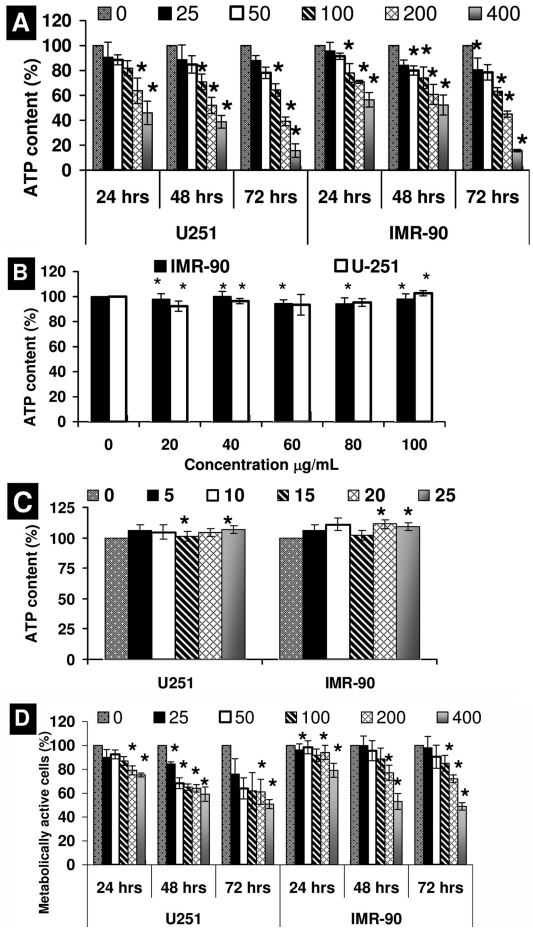

Figure 3. Data obtained from luminescent assay for Ag-np treated cancer cells (U251) and fibroblasts (IMR-90). Data represented as intracellular ATP content. The *y* axis represents the percent of reduction in ATP content compared to control. The *x* axis represents the time of incubation for different cell lines (U251, IMR-90). The different colors of the bars identify the concentration of Ag-np. (B) Data from starch alone controls, which after 72 h of incubation showed no significant cytotoxicity. (C) CellTiter blue cell viability assay shows a gradual drop in metabolically active cells. The *y* axis represents the percent of metabolically active cells present in the treated sample. The *x* axis represents the time of incubation for different cell lines (U251, IMR-90). The different colors of the bars identify the concentration of Ag-np. The values represent the mean ± standard deviation of three experiments; * denotes $P < 0.05$ as obtained using *student's t test*, where the statistical significance between untreated and Ag-np treated samples was analyzed for each concentration. Similar method was adopted for calculating starch treated cells, where untreated and starch treated cells were compared.

say. However, MTS assay was excluded from the test as Ag-np solution without the cells showed high absorbance readings. Hence, we concluded that the absorbance-based methods are not suitable for Ag-np treatment. The results from cell titer blue assays further confirmed metabolic arrest through the observed drop in mitochondrial activity (Figure 3D). The observations from cell titer blue assay led to the same inference as from ATP assay. Structural and functional damage of the mitochondria could result in metabolic arrest, followed by a decrease in ATP yield. A low ATP measure or mitochondrial activity does not always represent cell death, but could lead to metabolic inhibition in cells. In order to study the effect of starch in Ag-np, toxicity starch alone controls were also tested. However, starch did not result in any toxicity, which further confirmed that the observed toxicity is due to Ag-np alone. In summary, the viability assays were pointing at metabolic arrest rather than cell death. Hence, it is necessary to analyze the cell cycle to interpret the viability data fully.

Cytotoxicity of nanoparticles has been a robust research area in recent years. Many medically relevant nanoparticles such as gold and silver were investigated for their cytotoxicity aspect. Gold nanoparticles and nanorods showed no significant toxicity in HeLa cells,[21,22] while significant size-dependent toxicity was observed in fibroblast, epithelial cells, and melanoma cells.[23] Ag-np showed different degrees of *in vitro* cytotoxicity.[14,24] The cytotoxicity studies were limited by the fact that in most cases the dependence of time of exposure and surface functionalization remained unexplored. Despite the wide acceptance of starch as a suitable biocompatible capping agent, no study was reported on the toxicity of starch-capped nanoparticles. In this study, we have employed a time- and dose-dependent approach to evaluate the toxicity of starch-capped Ag-np. The biocompatibility data on starch indicated no cytotoxicity. We have used the most reliable and sensitive parameter, such as ATP content, to study the toxicity. The Ag-np used in this study have been purified extensively through repeated washing and centrifugation to remove traces of contaminants that may interfere with the assay. Unlike other nanoparticles, the Ag-np employed in our study exhibited a prominent metabolic arrest than cell death.

Role of Ag-np in Oxidative Stress. Earlier reports have emphasized the role played by oxidative stress in nanoparticle toxicity.[25] As discussed earlier, oxidative stress has specific effects in the cells, including oxidative damage to protein and DNA. To establish the role of oxidative stress as a decisive factor in starch-capped Ag-np toxicity, DCF-DA and DHE staining methods were performed. In the presence of reactive oxygen species (ROS), fluorescent intensity of the cells stained with dyes increased, which led to a right shift of the emission maximum. Untreated cells were used as standards to calculate the extent of ROS production by measuring the percentage of cells with increased fluorescence intensity. The analysis showed significant increase in hydrogen peroxide (Figure 4A) and superoxide production (Figure 4B) in cells treated with 25 and 50 μg/mL of Ag-np. The percent of gated cells from DCF-DA (Figure 4C) staining and HE staining (Figure 4D) was used for assessing the extent of ROS production. No significant increase was observed beyond 100 μg/mL. This effect may be due to exchange interactions between the unpaired electrons of the free radicals and the conduction band electrons of the metal nanoparticles. Such effect

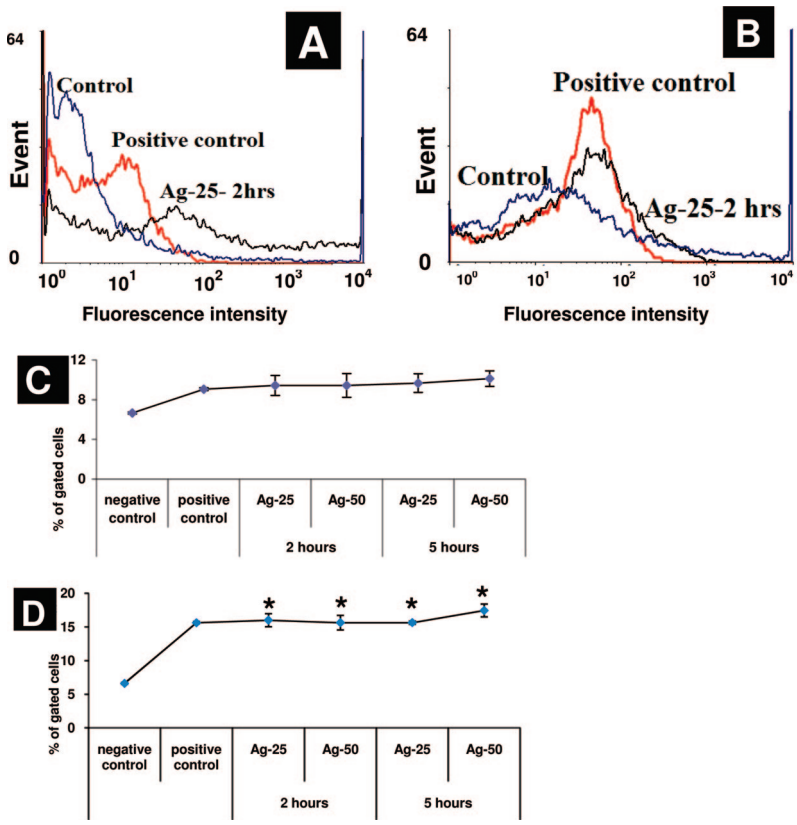

Figure 4. Histogram represents data from DCF-DA staining for detecting hydrogen peroxide production in the Ag-np treated fibroblasts (25 μg/mL) (A). Shift was independent of the time of incubation starting from 2 to 5 h of incubations. DHE staining (B) of the cells suggests superoxide production and increased ROS generation. The *x* axis represents the fluorescence intensity, and the *y* axis represents the number of cells collected (10000 cells). The graph represents the percent of gated cells for DCF-DA staining (C) and DHE staining (D) as obtained from the statistics generated by WinMDI 2.8 software. For DCF-DA staining along with untreated control, H_2O_2 treated cells were used as positive control. DDC was used as positive control for detecting superoxide production; * represents $P < 0.05$.

has been reported for gold nanoparticles.[26] It is possible that activation of a cellular antioxidant network had counterbalanced the effect of ROS.

Mitochondrial Respiratory Chain, Synthesis of ATP, and ROS Production. The decreased cellular ATP content could be an effect of damage caused to the mitochondrial respiratory chain. The mitochondrial damage is also indicated by the reduced dehydrogenase activity as measured by the reduction of resazurin to resofurin by CellTiter Blue viability assay. The root of mitochondrial dysfunction in toxicology is ROS production and subsequent oxidative stress. Oxidative stress is a common mechanism for the cell damage induced by nano- and ultrafine particles is well-documented.[25] Mechanical injury caused by nanoparticle depositions in mitochondria may be the reason for mitochondrial damage. Nanoparticles of various sizes and chemical compositions are shown to preferentially localize in mitochondria,[27] induce major structural damage, and contribute to oxidative stress.[25] Treatment of rat liver cell line with silver nanoparticles resulted in membrane damage, reduced glutathione levels, and increase in ROS production, indicating influence of nanoparticles on respiratory chain.[12] Majority of nanomaterials such as zinc oxide, carbon nanotubes, and silicon dioxide exert their toxic effects through oxidative stress,[28] similar to titanium dioxide nanoparticles reported earlier.[29] ROS was generated in the presence of Ag-np, which could explain the metabolic disturbances as well as other toxicological outcomes.

Mitochondria are the major sites of ROS production in the cell. During the oxidative phosphorylation, oxygen is reduced to water by addition of electrons in a controlled manner through the respiratory chain. Some of these electrons occasionally escape from the chain and are accepted by molecular oxygen to form the extremely reactive superoxide anion radical ($O_2^{-\bullet}$), which gets further converted to hydrogen peroxide (H_2O_2) and in turn may be fully reduced to water or partially reduced to hydroxyl radical ($OH^\bullet$), one of the strongest oxidants in nature.[30] Toxic agents increase the rate of superoxide anion production, either by blocking the electron transport or by accepting an electron from a respiratory carrier and transferring it to molecular oxygen without inhibiting the respiratory chain.[31] Inhibition of respiratory chain is expected to cause decrease in ATP synthesis. Deposition of Ag-np in mitochondria can alter normal functioning of mitochondria by disrupting the electron transport chain, ultimately resulting in ROS and low ATP yield. ROS are highly reactive and result in oxidative damage to proteins and DNA. Hence it is indispensable to investigate genome stability in cells with significantly higher ROS production.

It is possible that surface oxidation of Ag-np, upon contact with cell culture medium or proteins in the cytoplasm, liberates Ag^+ ions that could amplify the toxicity. Reactions between H_2O_2 and Ag-np are presumed to be one of the factors causing Ag^+ ions to release *in vivo*. Similar activity in cobalt and nickel nanoparticles has been reported. They release the corresponding ions that enhance toxicity.[32]

A possible chemical reaction involves

$$2Ag + H_2O_2 + 2H^+ \rightarrow 2Ag^+ + 2H_2O \quad E^0 = 0.17\ V$$

Half-reaction:

$$H_2O_{2(aq)} + 2H^+ + 2e^- \rightarrow 2H_2O_{(l)} \quad E^0 = +1.77\ V$$

$$2Ag^+_{(s)} \rightarrow 2Ag^+_{(aq)} + 2e^- \quad E^0 = 2(-0.8)\ V$$

H^+ ions are present in abundance inside the mitochondria where H^+ efflux is the main event (proton motive force) in ATP synthesis.

Toxicity of silver ions on *Escherichai coli* and other microbial cells has been studied[33] extensively, and the results can be extrapolated to mammalian cells due to the similarity in the respiratory chain. Various mechanisms have been suggested for the action of Ag^+ ion in the respiratory chain. Ag^+ ions have been shown to inhibit phosphate uptake and exchange in *E. coli*, which causes efflux of accumulated phosphate.[34] This effect is reversed by thiols, which could be due to the reversal of binding of Ag^+ to thiol containing proteins in the respiratory chain. Ag^+ ions were also shown to cause a leakage of protons through the membranes of *Vibrio cholerae*, thus causing the collapse of proton motive force, presumably by binding to membrane proteins.[35] NADH:ubiquinone reductase complex (Complex I) in *E. coli* contains two types of NADH dehydrogenases, both containing cysteine residues with high affinity for silver.[36,37] Both hydrogenases appear as possible sites for Ag^+ ion recognition.[36,38] Binding of Ag^+ to these low potential enzymes of the bacterial respiratory chain will result in an inefficient passage of electrons to oxygen at the terminal oxidase, causing production of large quantities of ROS and thus explaining the toxicity of ions to *E. coli* at submicromolar concentrations.[39] A consequence of interaction of Ag^+ ions with enzymes of the respiratory chain is sudden stimulation of respiration followed by cell death, due to uncoupling of respiratory control from ATP synthesis. Yet, prokaryotic cells and eukaryotic cells have entirely different physiological functions which determine sensitivity and survival rate upon exposure to nanoparticles. Eukaryotic cells have a prominent nucleus, a complex DNA repair mechanism, and cell cycle pathway to control cell death and survival, which are absent in prokaryotic cells.

Yamanaka *et al.*[40] studied the effect of Ag^+ ions on expression of various proteins in *E. coli* by proteomic analysis. Silver ions were assumed to penetrate through ion channels in the cell without causing damage to the membrane. Proteomic analysis of cells treated with Ag^+ ions showed a reduction in expression of ribosomal subunit S2, succinyl coenzyme (CoA) synthetase, and maltose transporter. The reduction in expression of ribosomal subunit S2 impairs the synthesis of other proteins, whereas reduction in synthesis of succinyl CoA synthetase and maltose transporter causes suppression of intracellular production of ATP, resulting in death of the cell. Hence, we believe that nanoparticle toxicity is multifactorial, where size, shape, surface functionalization and potential to release the corresponding metal ions could play pivotal roles.

Effect of Ag-np on Cell Cycle. Oxidative stress in Ag-np treated cells indicated the possibility of DNA damage where the early effect will be evidenced in cell cycle progression. Cells with damaged DNA will accumulate

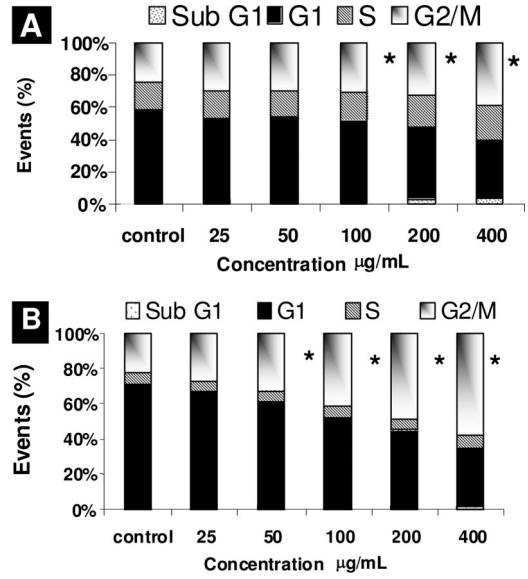

Figure 5. Ag-np treated U251 cells (A) showed a gradual increase in the S/G_2 population, and IMR-90 cells (B) showed a concentration-dependent G_2/M arrest. The statistical data are plotted as generated by WinMDI 2.8 software. Markers were set at regions of interest (subG_0, G_1, S, and G_2M), and the percent of cells (events) under each area was generated using the software; * represents $P < 0.05$. Histograms are included in the Supporting Information.

in gap1 (G_1), DNA synthesis (S), or in gap$_2$/mitosis (G_2/M) phase. Cells with irreversible damage will undergo apoptosis, giving rise to accumulation of cells in subG_1 phase.[41] Thus toxicity studies were further extended to cell cycle analysis to detect parameters such as apoptosis, cell cycle arrest, and evidence of DNA damage.

The influence of nanoparticles on the cell cycle was analyzed by subjecting the nanoparticle treated cells to flow cytometry. Statistical data from raw histograms (Supporting Information) were extracted using WinMDI software, and the percent of cells in each phase of the cell cycle was compared with that of controls. Both cell types showed a concentration-dependent G_2 arrest (U251, Figure 5A, and IMR-90, Figure 5B) which was observed as an increase in cell population in G_2/M phase compared to control. The lowest concentration of nanoparticles tested (25 μg/mL) marked the onset of G_2/M arrest. As the concentration of Ag-np was increased to 400 μg, there was a massive increase (approximately 30%) in G_2 population. In controls, major cell population was observed in G_1 phase, whereas in Ag-np treated cells, a decrease in G_1 population accompanied by an increase in G_2/M population was detected. The proportion of cells in S phase was less affected as compared to the G_2/M population. No significant apoptosis was observed, as indicated by the absence of cell population in subG_1.

Apoptosis and Necrosis. To assess the extent and mode of cell death, annexin-V staining was carried out. Statistical data were extracted from the dot plots (Supporting Information Figure S4B) using WinMDI software, based on the percentages of unstained cells (viable

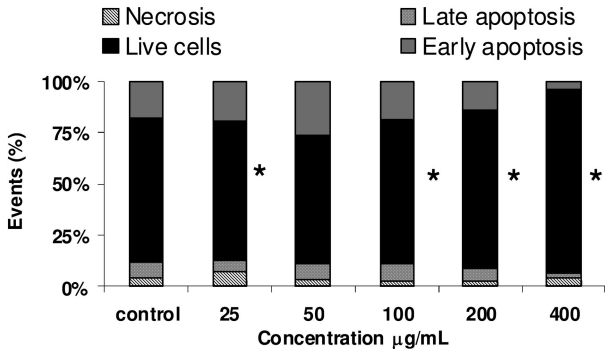

Figure 6. Annexin-V staining of normal fibroblasts to detect the mode of cell death indicated that a small percentage of cells are undergoing cell death, and a major population is viable. The statistical data are plotted as generated by WinMDI 2.8 software. The percent of cells stained with PI alone is represented as necrotic cells, whereas percent of cells stained with FITC alone represents early apoptosis. Cells at final stages of apoptosis take up both stains. The details of the experiments with cancer cells are included in Figure S4 in the Supporting Information; * represents $P < 0.05$.

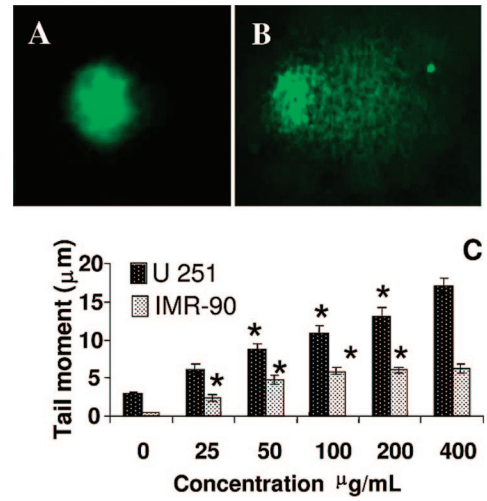

Figure 7. Comet analysis: untreated (A) and Ag-np treated (B) cancer cells stained by SYBR green (conc. 400 μg/mL). (C) Represents the tail moments of DNA (μm). Fibroblasts exhibited a concentration-dependent increase in DNA damage up to 100 μg, above which the values remained constant, whereas cancer cells showed a steady increase; * represents $P < 0.05$.

cells), and those with red fluorescent labels (necrotic cells), green labels (apoptotic cells), and dual stained cells (late apoptosis) were analyzed. The data from the annexin-V staining experiment indicated that only a small percentage of cells was undergoing apoptosis and necrosis at higher concentrations of Ag-starch nanoparticles (Figure 6). There was an increase (5−9% with respect to control) in the apoptotic cell population from 25 to 100 μg/mL for fibroblasts, which could be attributed to the observed ROS production, while 16% (±5) of cell death observed was due to late apoptosis and necrosis. Induction of apoptosis specifically in low doses of nanoparticles accompanied by proliferation arrest at high concentrations suggests differential sensitivity of nanoparticle concentrations. It could also be interpreted as a situation where cells sustain DNA damage and gain resistance to cell death. A concentration-dependent increase in DNA damage and G_2/M arrest establishes that DNA damage is increasing with concentration. Recent reports have identified apoptosis as a major mechanism of cell death in exposure to nanomaterials.[14,23] However, conflicting results support involvement of additional parameters in nanoparticle-mediated cell death, which requires detailed study.[22,24] Future experiments will be designed to identify the molecular mechanisms underlying nanoparticle-mediated cell death. DNA fragmentation analysis was carried out to study DNA fragmentation characteristic of late apoptosis. No laddering patterns were observed in the gel, which confirmed the absence of late apoptosis where nuclear fragmentation occurs (Figure S3, Supporting Information). Absence of massive apoptosis and necrosis at higher concentrations of Ag-np accompanied by G_2/M arrest indicated a retarded cell proliferation. This inference is supported by the cell cycle and genotoxicity data.

Genotoxicity of Ag-np. DNA damage by Ag-np was further studied using comet assay and cytokinesis-blocked micronucleus assay. Chromosome abnormalities are a direct consequence of DNA damage such as double-strand breaks and misrepair of strand breaks in DNA, resulting in chromosome rearrangement. Micronuclei (MN) were formed in dividing cells from chromosome fragments or whole chromosomes that were unable to engage with the mitotic spindle during mitosis.[42]

Extensive and dose-dependent damage to DNA was observed after treatment of the cells with Ag-np. Comet assay of Ag-np treated cells showed a concentration-dependent increase in tail momentum (Figure 7B) as compared to control cells (Figure 7A), which gave the extent of DNA damage (Figure 7C). A comet-like tail implies presence of a damaged DNA strand that lags behind when electrophoreses was done with an intact nucleus. The length of the tail increases with the extent of DNA damage. Tail momentum of control DNA was compared with nanoparticle treated cells, and extent of damage was assessed. An increase in DNA damage with increase in nanoparticle concentration was observed in cancer cells, whereas the fibroblasts showed no further increase in DNA damage beyond a nanoparticle concentration of 100 μg/mL.

In addition, the cytokinesis-blocked micronucleus assay results further corroborated the chromosomal breaks in Ag-np treated cells (Figure 8B) as compared to the untreated cells (Figure 8A). Extent of DNA damage was much higher in cancer cells as compared to fibroblasts, and significant numbers of micronuclei were formed in cancer cells than fibroblasts (Figure 8C).

Few apoptotic or necrotic cells were observed during the CBMN analysis, and annexin-V staining showed only a few apoptotic and necrotic cells. As described

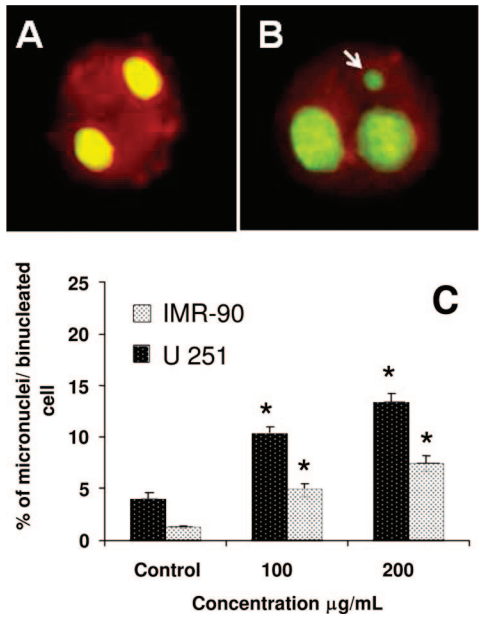

Figure 8. Micronucleus analysis of untreated (A) and Ag-np (100 μg/mL) treated (B) fibroblasts showing binucleated cell. White arrow (B) indicates the micronucleus formed among the binucleated cells. Data from MNA (C) show chromosomal aberrations. The data represent 1000 binucleated cells for U251 and 700 binucleated cells for fibroblasts; * represents $P < 0.05$.

earlier, presence of Ag-np caused the formation of ROS and reduction in ATP content. ROS are considered to be the major source of spontaneous damage to DNA. Oxidative attack on the DNA results in mutagenic structures such as 8-hydroxyadenine and 8-hydroxyguanine, which induces instability of repetitive sequences. The chemical reactions that bring about such mutations are based on the formation of highly reactive and short-lived hydroxyl radical ($OH^{\bullet}$) in close proximity to DNA.[43] ROS-mediated genotoxicity has been previously observed for metal oxide nanoparticles.[28] This is the first study that provides quantitative measurements of DNA damage and chromosomal aberrations in Ag-np treated cells.

Further damage may occur through single- and double-strand breaks, inter- and intrastrand cross-linking *etc*. On the other hand, silver ions have been shown to interact with DNA and RNA under *in vitro* conditions.[44] Ag^+ ions form a type I complex by binding to N7 of guanine or adenine, and in a type II complex, it forms interstrand AT and GC adducts without causing much change in the conformation of DNA. Hossain and Huq[45] proposed stabilization of DNA by Ag^+ ions by studying the binding of Ag^+ ions to plasmid and chromosomal DNA in *in vitro* condition. However, they found that, in the presence of ascorbate, Ag^+ ions caused significantly more damage to DNA than the ascorbate alone. It is expected that Ag^+ ion catalyzed oxidation of ascorbate anion by molecular oxygen causes the formation of free radicals, which could damage DNA.

DNA Damage, Cellular ATP Content, and Cell Cycle Arrest. In eukaryotic cells, DNA damage caused the arrests of cell cycle progression at the G2/M boundary, allowing cells extra time to repair damage prior to segregation of chromosomes. The DNA repair machinery must access the nucleosome in order to carry out the repair. Two classes of enzymes are involved in regulating the accessibility to chromatin, one modifying the core group histone amino acids and the other consisting of large multisubunit complexes known as chromatin remodelers which use the energy from ATP hydrolysis to weaken the interactions between histones and the surrounding DNA. The reduction in ATP content (Figure 3) after Ag-np treatment could affect the DNA repair, as ATP is required for a cascade of events requiring phosphorylation of several proteins taking part in repair of DNA damage.[46]

The role of ATP in cell cycle arrest was studied by Sweet *et al.*[47] through specifically inhibiting the mitochondrial production of ATP. It was shown that a small reduction in the cellular level of ATP induced a significant increase in the G_1 cell population, while further decrease (up to 35%) elicited a G_2/M accumulation followed by the onset of cytotoxicity. This suggests that the checkpoints regulating passage through cell cycle events are sensitive to alteration in the ATP status of the cell.

The extensive damage of DNA measured by comet assay and CBMN assay was reflected into the arrest of the IMR-90 and U251 cells in the S and G_2/M phases. The number of cells in the G_2/M phase increased with increasing dose of the silver nanoparticles. Cell cycle arrest provides enough time for the cells to repair the damaged DNA. Similar results were reported for carbon-black nanoparticles.[48] The cells treated with carbon-black nanoparticles suffered DNA damage which led to cell cycle arrest. To date, no such studies were conducted for silver nanoparticles, and here we attempt to unveil the effect of Ag-np on the cell cycle. The DNA damage caused by Ag-np to the U251 cells was much more extensive than that to the IMR-90 cells and correlated well with the steeper increase in the number of cells in the G_2/M phase with concentration of Ag-np. The increased sensitivity of U251 cells to DNA damage could be due to the impaired repair pathways. In fact, current cancer therapy relies heavily on DNA damaging agents to induce programmed cell death in cancer cells.

Transmission Electron Microscopy (TEM) of Cell Sections. In order to study the biodistribution of the Ag-np, TEM analyses of the cancer cells treated with 100 μg/mL of nanoparticles were performed. Untreated cells showed no abnormalities (Figure 9A), whereas Ag-np treated cells showed endosomes near the cell membrane with a large number of nanoparticles inside (Figure 9B). The nanoparticles were found to distribute throughout the cytoplasm, inside lysosomes and nucleus (Figure 9C).

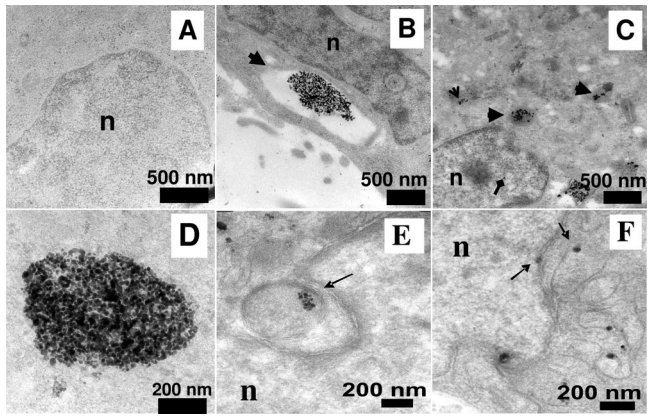

Figure 9. TEM images of ultrathin sections of cells. Untreated cells showed no abnormalities (A), whereas cells treated with Ag-np showed large endosomes near the cell membrane with many nanoparticles inside (B). Electron micrographs showing lysosomes with nanoparticles inside (thick arrows) and scattered in cytoplasm (open arrow). Diamond arrow shows the presence of the nanoparticle in the nucleus (C). Magnified images of nanogroups showed that the cluster is composed of individual nanoparticles rather than clumps (D). Image shows endosomes in cytosol that are lodged in the nuclear membrane invaginations (E) and the presence of nanoparticles in mitochondria and on the nuclear membrane (F).

Clumps of nanoparticles found inside endosomes and in cytoplasm were similar to nanoaggregates. However, magnified images showed the presence of individual nanoparticles within the clump (Figure 9D).We also observed large endosomes with nanoparticles in the cytoplasm of the cells and near the cell and nuclear membrane, which suggested that nanoparticles were entering the cells through endocytosis rather than diffusion. The cytoplasm of the cells showed multiple endosomes with engulfed nanoparticles, and such endosomes were also observed near the nuclear membrane (Figure 9E). The nanoparticles were also seen deposited inside other organelles such as mitochondria (Figure 9F).

Nanoparticle deposition was observed in the nucleus and nucleolus. The nuclear envelope has multiple pores (nuclear pore complexes) with an effective diameter of 9−10 nm, through which transport of proteins takes place. Owing to their small size, Ag-np could be readily diffused into the nucleus through the pores. The Ag-np or some of the Ag^+ ions inside the cell nucleus may bind to the DNA and augment the DNA damage caused by the ROS. Small vesicles carrying nanoparticles were observed to be in contact with invaginations of nuclear membrane (Figure 9E). The cytoplasm of the cells showed heavy deposition of nanoparticles, outside the vesicles. A possible reason could be the damage to the heavy nanoparticle loaded endosomes, resulting in deposition of the particles in cytoplasm. The cells with a small number of nanoparticles are believed to survive longer. Recent reports have established a similar mechanism, whereby gold nanoparticles were taken up by the cells through clathrin and caveoli mediated endocytosis.[49] The report established the influence of surface chemistry where different surface functionalization resulted in distinct uptake pathways. Similar properties can be expected for silver nanoparticles. However, no nuclear deposition was observed in unmodified gold nanoparticles, and here we illustrate the intracellular distribution of Ag-np. The tendency of the nanoparticles to accumulate in the nuclei of the cells is assumed to be associated with the small size which allows them to diffuse freely through an uclear pore complex as reported for gold and silica nanoparticles.[50] However, detailed investigation must be done to study if small vesicles carrying nanoparticles lodged in the nuclear invaginations play a role in transferring nanoparticles to the nucleus. Also, the mechanism of deposition of nanoparticles in mitochondria remains unknown. The current evidence from electron micrographs sheds light on the endocytic pathway of nanoparticle uptake. There are different types of active endocytic pathways such as receptor mediated endocytosis (clathrin or caveoli mediated) and macropinocytosis.[51] A detailed study will be conducted to unravel the mechanism involved in Ag-np uptake. Elemental mapping of cell sections using STEM confirmed the distribution of Ag-np within the cell (Figure 10A). The embedded Ag-np were located and represented as red color dots (Figure 10B). Scanning transmission electron micrographs and elemental mapping of the cell sections further confirmed the TEM observations.

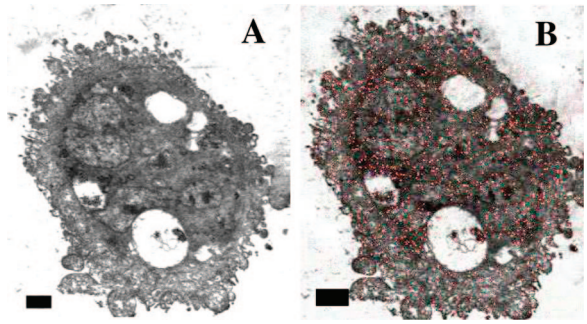

Figure 10. (A) STEM images of nanoparticle treated cell sections. (B) Superimposed image of nanoparticle treated cells with elemental mapping. Red spots indicate presence of silver. Images of the cell and mapping of the same cell were captured using a field emission scanning electron microscope. The images were merged using Image Merger version 1.0.20. Scale bar = 2 μm.

Ag-np were found to be toxic to both human lung fibroblast (*e.g.*, IMR-90) and the human glioma (*e.g.*, U251) cell lines used in the study. A change in morphology of the cells was observed upon Ag-np treatment as the first indication of toxicity. Electron micrographs confirmed a significant number of nanoparticles in vital organs such as mitochondria and nucleus. Significant decrease in cell viability was observed, probably as a result of reduction in ATP production, generation of reactive oxygen species (ROS), and damage to the mitochondrial respiratory chain. The ROS production is believed to be the trigger for DNA damage, followed by cell cycle arrest at G_2/M. The cells arresting at G_2/M are

not undergoing massive apoptosis or necrosis, and no fragmented nuclei or necrotic cells were observed in CBMN analysis. The comet and CBMN assays demonstrated extensive DNA damage to both cell lines, the U251 cells being much more vulnerable than the IMR-90 cells. Hence we speculate that the accumulation of cells at the G_2/M interface is associated with DNA repair which could lead to cell death or survival at a later stage. All the data taken together suggest that silver nanoparticles at the range of concentrations used resulted in G_2/M arrest in the cells, which might lead to cell death if repair pathways were unsuccessful.

CONCLUSION

Here a genotoxic and cytotoxic approach was employed to elucidate the activity of Ag-np. The results from our research indicated mitochondrial dysfunction, induction of ROS by Ag-np which in turn set off DNA damage and chromosomal aberrations (comet assay and CBMN analysis). DNA damage and chromosomal aberrations are believed to be the prime factors resulting in cell cycle arrest. The fate of the cells arrested at G_2/M interface was analyzed by annexin-V PI assay which showed no massive cell death, suggesting involvement of an active DNA repair pathway. The cells which successfully repair the damage will re-enter the cell cycle, and those with massive damage will not be able to repair the DNA effectively and undergo apoptosis at a later stage. We conclude that even a small dose of Ag-np has the potential to cause toxicity as analyzed by an array of cyto- and genotoxicity parameters. The DNA damage, chromosomal aberrations, and cell cycle arrest raise the concern about the safety associated with applications of the Ag-np. The present study concludes that Ag-np are cytotoxic, genotoxic, and antiproliferative. As a general rule, the DNA damaging agents have the potential to cause genome instability, which is a predisposing factor in carcinogenesis. The outcome of the nuclear deposition of Ag-np is unknown at this point, however, it is likely to have adverse effects. Future application of Ag-np as an antiproliferative agent could be limited by the fact that it is equally toxic to normal cells. Hence it is imperative that the biological applications employing Ag-np should be given special attention besides embracing the antimicrobial potential. Further studies must be conducted in this field to achieve the deeper understanding of Ag-np toxicity.

MATERIALS AND METHODS

The particle synthesis was carried out using the standard procedure through reduction of silver nitrate. All experiments were done in a clean atmosphere to eliminate the chances of endotoxin contamination[52] that may interfere with the toxicity profile of the nanoparticle. All chemicals used for nanoparticle synthesis were purchased from Sigma-Aldrich.

Preparation of Starch-Capped Ag-np. Starch-coated silver nanoparticles were synthesized by a method reported by Raveendran *et al.*[19] The choice of capping agent was done based on the stability of nanoparticles in cell culture medium. Starch-capped nanoparticles showed lesser degree of agglomeration even at high concentrations compared to the silver nanoparticles capped with polyvinyl alcohol and proteins. Furthermore, the choice of capping agent is important since the properties of nanoparticles can be significantly altered through surface modification. The distribution of nanoparticles in the body is strongly influenced by its surface characteristics. The hydrophilic nature of starch as compared to organic polymers could enhance the water dispersion and hence stability in cell culture medium. Moreover, using starch as the capping agent removed the need of other organic solvents, or capping agents, which are toxic to the cells. Additionally, our experiments showed that starch controls were not cytotoxic to the cells under study. Briefly, soluble starch from potatoes (0.28 g) was dissolved in 10 mL of boiling ultrapure water and filtered using a 0.2 μm syringe filter (Sartorius, Goettingen, Germany). Silver nanoparticles were synthesized by reducing silver nitrate solution (1 mM), using sodium borohydride (0.03 g) followed by the addition of the filtered starch solution, under constant stirring at 70 °C. The color of the solution changed to dark brown with time, indicating nanoparticle formation, and stirring was continued for an additional 2 h. The nanoparticle suspension was centrifuged at 18 000 rpm for 1 h to pellet nanoparticles. The pellets were further washed in ultrapure water to remove traces of unbound starch. The dry pellet obtained after the lyophilization of the centrifuged nanoparticles was dissolved in ultrapure water using sonication. The size of the nanoparticles was determined by TEM (Figure 1A) analysis and ultraviolet (UV) absorption spectrum (Figure 1B), using pure nanoparticle suspensions reconstituted from the lyophilized powder. A size distribution histogram was extracted from Figure 1A using Gatan digital micrograph software (Gatan Inc., CA). Electron micrographs of Ag-np are included in the Figure S1 in the Supporting Information.

Cell Culture and Nanoparticle Treatment. Cell lines were purchased from commercial sources, IMR-90: Coriell Cell Repositories, USA; U251 cells: Dr. Masao Suzuki, National Institute of Radiological Sciences, Chiba, Japan. Human glioblastoma cells (U251) were maintained in Dulbecco's modified eagles medium (DMEM, Sigma-Aldrich, St. Louis, MO) supplemented with 10% fetal bovine serum (FBS, GIBCO, Invitrogen, Grand Island, NY) and 1% penicillin streptomycin (Gibco, Invitrogen, Grand Island, NY). Normal human fibroblasts (IMR-90, at passage 20 $\pm$ 3) were maintained in modified eagles medium with glutamine (MEM, Gibco, Invitrogen, Grand Island, NY) supplemented with 15% FBS, 1% each of penicillin streptomycin, nonessential amino acids, vitamins, and 2% essential amino acids (Gibco, Invitrogen, Grand Island, NY). Cells were maintained in a 5% CO_2 incubator at 37 °C.

Stock solutions of nanoparticles (5 mg/mL) were prepared in sterile distilled water and diluted to the required concentrations using the cell culture medium. Appropriate concentrations of Ag-np stock solution were added to the cultures to obtain respective concentration of Ag-np and incubated for 48 h. Following Ag-np treatment, the plates were observed under a light microscope (Olympus CK 40) to detect morphological changes and photographed using an Olympus C7070WZ camera.

Transmission Electron Microscopy (TEM) of Ag-np Treated Cells. Ultrathin sections of the cells were analyzed using TEM to reveal the distribution of nanoparticles. Briefly, the cells (1.5×10^6 cells) were treated with Ag-starch nanoparticles (net concentration of 100 μg/mL) for 48 h. At the end of the incubation period, culture flasks were washed many times with phosphate buffer to get rid of excess unbound nanoparticles. Cells were trypsinized and washed 4−5 times in phosphate buffer and fixed in 2.5% glutaraldehyde for 2 h. Fixed cells were washed 3 times with phosphate buffer. Post-fixation staining was done using 1% osmium tetroxide for 1 h at room temperature. Cells were washed well and dehydrated in alcohol (40, 50, 70, 80, 90, 95, and 100% ethanol) and treated twice with propylene oxide for 30 min each, followed by treatment with propylene oxide, spurr's low viscos-

ity resin (1:1), for 18 h. Cells were further treated with pure resin for 24 h and embedded in beem capsules containing pure resin. Resin blocks were hardened at 70 °C for 2 days. Ultrathin sections (70 nm) were cut using Reichert Jung Ultracut. The sections were stained with 1% lead citrate and 0.5% uranyl acetate and analyzed under JEOL JEM 2010F. The presence of nanoparticles was confirmed by the electron dispersive X-ray analysis (EDX, Figure S2 in the Supporting Information).

Scanning Transmission Electron Microscopy (STEM). Scanning transmission electron microscopy (STEM) and the elemental mapping of cell sections were done to elucidate the distribution pattern of nanoparticles. The sections prepared for the TEM analysis were employed for STEM study. The instrument performed elemental mapping by labeling silver as red dots in the image captured. The analysis was done using JEOL JSM 6701F at an accelerating voltage of 25 kV.

Cell Viability Assay. The viability of Ag-np treated cells was measured using Cell-Titer glow luminescent cell viability assay (Promega, Madison, WI) following manufacturer's instructions. This assay is a homogeneous method for determining the number of viable, metabolically active cells in a culture based on quantification of the ATP concentration. The procedure involves addition of an equal volume of reagent to the medium in test wells, which in a single step generates a luminescent signal proportional to the concentration of ATP present in cells. The reagent contains detergents to break the cell membrane, causing ATP release in the medium and ATPase inhibitors to stabilize the released ATP. The assay is based on the conversion of beetle luciferin to oxyluciferin by a recombinant luciferase in the presence of ATP. The observed luminescence is proportional to the quantity of ATP in cells. The experiments were performed in white opaque walled 96-well plates (Corning, Costar, NY). Additional controls were included in the test to rule out autoluminescence and quenching by silver nanoparticles. For the ATP assay, 1×10^4 cells per well were plated and treated with different concentrations of nanoparticles (25, 50, 100, 200, and 400 μg/mL) for 24, 48, and 72 h. The dependence of toxicity on purity of nanoparticles was studied using the supernatants from the last centrifugation step. The supernatant (50 mL) obtained after removing the nanoparticle pellet was concentrated by lyophilization and reconstituted in 1 mL of sterile water. Different volumes of the stock solution (0, 5, 10, 15, 20, and 25 μL) were dispensed in to 100 μL of medium in 96-well plates and incubated for 48 h.

Mitochondrial Function Cell Titer Blue Cell Viability Assay. Cell titer blue cell viability assay (Promega, Madison, WI) is a fluorimetric measurement of the metabolically active cells in a culture. The mitochondrial and microsomal enzymes reduce resazurin in the reagent to resorufin, which are highly fluorescent. Cells were seeded at a density of 1×10^4 cells per well, in black opaque walled 96-well plates (Corning, Costar, NY) and treated with Ag-np as described for ATP assay. A time-dependent study was conducted employing different incubation period (24, 48, and 72 h) after nanoparticle addition. The experiments were carried out as per supplier's instructions.

Cell Cycle Analysis. Cell cycle analysis was carried out by staining the DNA with propidium iodide (PI) followed by flow cytometric measurement of the fluorescence. Approximately 4×10^5 U251 cells and 8×10^5 IMR 90 cells were placed in 100 mm tissue culture dish (Falcon, Franklin Lakes, NJ, USA). Following the Ag-np treatments for 48 h (concentrations employed were similar as in viability studies), the medium was removed and stored. Cells were washed in 1X phosphate buffered saline (PBS, 1st Base, Singapore) trypsinized, harvested in the stored medium, and centrifuged. The pellet was washed in PBS, fixed in ice-cold ethanol (70%), and stored at −20 °C. Before flow cytometry analysis, cells were washed in PBS and stained with propidium iodide (PI) in RNase (40 μg/mL PI and 100 μg/mL RNase A) and incubated at 37 °C for 30 min, followed by incubation at 4 °C until analysis. Flow cytometry analysis was performed using Epics Altra (Beckman and Coulter) at an excitation wavelength of 488 nm and emission wavelength of 610 nm. Data collected for 2×10^4 cells was analyzed using WinMDI 2.8 software.[53]

Annexin-V Staining. Annexin-V staining was performed to differentiate apoptosis from necrotic cell death induced by Ag-np. Annexin-V has a high affinity for phosphotidyl serine, which is translocated from the inner to the outer leaflet of the plasma membrane at an early stage of apoptosis. Its conjugation with the fluorescent probe FITC facilitates measurement by flow cytometric analysis. Use of propidium iodide (PI) staining helps distinguish between apoptosis and necrosis due to difference in permeability of PI through the cell membranes of live and damaged cells. Cell number, concentrations, and culture conditions were similar to cell cycle analysis. Treated cells were harvested and washed twice in PBS. The staining was carried out as per manufacturer's instruction (annexin-V FITC apoptosis detection kit, Sigma-Aldrich, St. Louis, MO). Data analyses were done using WinMDI software.

Detection of Reactive Oxygen Species (ROS) Production. The generation of hydrogen peroxide and superoxide radical was monitored by employing 2′,7′- dichlorodihydrofluorescein diacetate (DCF-DA, Invitrogen, Grand Island, NY) staining[54] and dihydroethidium (DHE, Sigma-Aldrich, St. Louis, MO) staining,[55] respectively. DCF-DA is nonfluorescent unless oxidized by the intracellular ROS. Dihydroethidium is blue fluorescent in the reduced form, which upon oxidation by superoxide radical emits red fluorescence. Dose- and time-dependent measurements of the generation of reactive oxygen species were done by incubating one million cells with Ag-np (25, 50, 100, and 200 μg) for 2 and 5 h, followed by staining with 2 μM DHE and 10 μM DCF-DA for 15 min at 37 °C. Hydrogen peroxide treated cells (0.09% H_2O_2) were used as positive control for DCF-DA analysis, whereas diethyldithiocarbamic acid (DDC) at a concentration of 100 μM (2 h at 37 °C) was used as positive control for DHE staining. DDC is a strong inhibitor of superoxide dismutase activity in cells. Cells were then washed twice in serum-free medium and analyzed using Epics Altra flow cytometer (Beckman & Coulter) at an excitation wavelength of 488 nm and emission wavelengths of 530 and 610 nm for DCF-DA and HE, respectively. The concentrations were chosen based on the viability data. For each sample, 1×10^4 cells were collected (Epics Altra, Beckman Coulter), and data were analyzed using WinMDI 2.8 software.

Cytokinesis-Blocked Micronucleus Assay (CBMN). Cytokinesis-blocked micronucleus assay (CBMN) measures the chromosomal breakage that occurs due to exposure to toxic agents.[42] Cell density was similar to cell cycle analysis. The cells were treated with two different concentrations of Ag-np (100 and 200 μg) for 48 h followed by further incubation for 22 h with cytochalasin B (Sigma-Aldrich, St. Louis, MO, 5 μg/mL). The analysis was performed according to a reported procedure.[56] Cells were harvested and treated with ice cold KCl and centrifuged immediately. The pellet was fixed in Carnoy's fixative (3:1 methanol/acetic acid), and a few drops of formaldehyde were added to preserve the cytoplasm. The cells were aged for at least 4 days at 4 °C, streaked on clean glass slides, and dried. The slides were then stained with acridine orange (30 μg/mL), which differentially stains the nucleus and cytoplasm.[57] One thousand binucleated cells were scored, and the number of micronuclei was recorded. The IMR 90 cells had approximately 700 binucleated cells.

Alkaline Single-Cell Gel Electrophoresis (Comet Assay). Alkaline single-cell gel electrophoresis (Comet assay) detects DNA damage through electrophoresis[58] and subsequent staining in SYBR green dye. Treated cells were harvested and washed twice in PBS before resuspending in Hank's balance salt solution (HBSS, Sigma-Aldrich, St. Louis, MO) with 10% dimethyl sulfoxide (DMSO, AppliChem GmbH, Ottoweg, Darmstadt, Germany) and EDTA (1st Base, Singapore). The cells were embedded in 0.8% low melting agarose (Pronadisa, Spain) on comet slides (Trevigen, Gaithersburg, MD) and lysed in prechilled lysis solution (2.5 M NaCl, 0.1 M EDTA, 10 mM Tris base, pH 10) with 1% Triton X (Trevigen, Gaithersburg, MD) for 1 h at 4 °C. Cells were then subjected to denaturation in alkaline buffer (0.3 M NaCl, 1 mM EDTA) for 40 min in the dark at room temperature. Electrophoresis was performed at 25 V and 300 mA for 20 min. The slides were immersed in neutralization buffer (0.5 M Tris-HCl, pH 7.5) for 15 min followed by dehydration in 70% ethanol. The slides were air-dried and stained with SYBR green dye. The tail moments of the nuclei were measured as a function of DNA damage. Analysis was done using comet imager v1.2 software (Metasystems GmbH, Altlussheim, Germany), and 50 comets were analyzed per concentration.

Statistical analyses of the values for all experiments are expressed as mean ± standard deviation of three independent experiments. The data were analyzed using *Student's t test* (Microsoft Excel, Microsoft Corporation, USA) where statistical significance was calculated using untreated (control) and nanoparticle treated samples and those with P value <0.05 are considered as significant.

Acknowledgment. This work was supported by the Office of Life Sciences (OLS) at the National University of Singapore (NUS). We acknowledge facilities support by the NUS-Nanoscience and Nanotechnology Initiative (NUSNNI), Department of Chemistry and Department of Physiology. The authors thank L. V. Bindhu and S. Shubhada for their help with the manuscript.

Supporting Information Available: Additional details of experiments and results are included. This material is available free of charge *via* the Internet at http://pubs.acs.org.

REFERENCES AND NOTES

1. Kreuter, J.; Gelperina, S. Use of Nanoparticles for Cerebral Cancer. *Tumori.* **2008**, *94*, 271–277.
2. Yoon, K. Y.; Hoon, B. J.; Park, J. H.; Hwang, J. Susceptibility Constants of *Escherichia coli* and *Bacillus subtilis* to Silver and Copper Nanoparticles. *Sci. Total Environ.* **2007**, *373*, 572–575.
3. Tan, W. B.; Jiang, S.; Zhang, Y. Quantum-Dot Based Nanoparticles for Targeted Silencing of HER2/neu Gene *via* RNA Interference. *Biomaterials* **2007**, *28*, 1565–1571.
4. Su, J.; Zhang, J.; Liu, L.; Huang, Y.; Mason, R. P. Exploring Feasibility of Multicolored CdTe Quantum Dots for *In Vitro* and *In Vivo* Fluorescent Imaging. *J. Nanosci. Nanotechnol.* **2008**, *8*, 1174–1177.
5. Lok, C. N.; Ho, C. M.; Chen, R.; He, Q. Y.; Yu, W. Y.; Sun, H.; Tam, P. K.; Chiu, J. F.; Che, C. M. Proteomic Analysis of the Mode of Antibacterial Action of Silver Nanoparticles. *J. Proteome Res.* **2006**, *5*, 916–924.
6. Gogoi, S. K.; Gopinath, P.; Paul, A.; Ramesh, A.; Ghosh, S. S.; Chattopadhyay, A. Green Fluorescent Protein-Expressing *Escherichia coli* as a Model System for Investigating the Antimicrobial Activities of Silver Nanoparticles. *Langmuir* **2006**, *22*, 9322–9328.
7. Kim, J. S.; Kuk, E.; Yu, K. N.; Kim, J. H.; Park, S. J.; Lee, H. J.; Kim, S. H.; Park, Y. K.; Park, Y. H.; Hwang, C. Y.; *et al.* Antimicrobial Effects of Silver Nanoparticles. *Nanomedicine* **2007**, *3*, 95–101.
8. Samuel, U.; Guggenbichler, J. P. Prevention of Catheter-Related Infections: The Potential of a New Nano-Silver Impregnated Catheter. *Int. J. Antimicrob. Agents* **2004**, *23*, S75–S78.
9. Chen, J.; Han, C. M.; Lin, X. W.; Tang, Z. J.; Su, S. J. Effect of Silver Nanoparticle Dressing on Second Degree Burn Wound. *Zhonghua Wai Ke. Za Zhi.* **2006**, *44*, 50–52.
10. Lesniak, W.; Bielinska, A. U.; Sun, K.; Janczak, K. W.; Shi, X.; Baker, J. R., Jr.; Balogh, L. P. Silver/Dendrimer Nanocomposites as Biomarkers: Fabrication, Characterization *In Vitro* Toxicity, and Intracellular Detection. *Nano Lett.* **2005**, *5*, 2123–2130.
11. Braydich-Stolle, L.; Hussain, S.; Schlager, J. J.; Hofmann, M. C. *In Vitro* Cytotoxicity of Nanoparticles in Mammalian Germline Stem Cells. *Toxicol. Sci.* **2005**, *88*, 412–419.
12. Hussain, S. M.; Hess, K. L.; Gearhart, J. M.; Geiss, K. T.; Schlager, J. J. *In Vitro* Toxicity of Nanoparticles in BRL 3A Rat Liver Cells. *Toxicol. In Vitro* **2005**, *19*, 975–983.
13. Arora, S.; Jain, J.; Rajwade, J. M.; Paknikar, K. M. Cellular Responses Induced by Silver Nanoparticles: *In Vitro* Studies. *Toxicol. Lett.* **2008**, *179*, 93–100.
14. Hsin, Y. H.; Chen, C. F.; Huang, S.; Shih, T. S.; Lai, P. S.; Chueh, P. J. The Apoptotic Effect of Nanosilver is Mediated by a ROS- and JNK-Dependent Mechanism Involving the Mitochondrial Pathway in NIH3T3 Cells. *Toxicol. Lett.* **2008**, *179*, 130–139.
15. Sung, J. H.; Ji, J. H.; Yoon, J. U.; Kim, D. S.; Song, M. Y.; Jeong, J.; Han, B. S.; Han, J. H.; Chung, Y. H.; Kim, J.; *et al.* Lung Function Changes in Sprague-Dawley Rats After Prolonged Inhalation Exposure to Silver Nanoparticles. *Inhal. Toxicol.* **2008**, *20*, 567–574.
16. Asharani, P. V.; Wu, Y. L.; Gong, Z.; Valiyaveettil, S. Toxicity of Silver Nanoparticles in Zebrafish Models. *Nanotechnology* **2008**, *19*, 1–8.
17. Singh, S.; Nalwa, H. S. Nanotechnology and Health Safety-Toxicity and Risk Assessments of Nanostructured Materials on Human Health. *J. Nanosci. Nanotechnol.* **2007**, *7*, 3048–3070.
18. Nel, A.; Xia, T.; Madler, L.; Li, N. Toxic Potential of Materials at the Nanolevel. *Science* **2006**, *311*, 622–627.
19. Raveendran, P.; Fu, J.; Wallen, S. L. Completely "Green" Synthesis and Stabilization of Metal Nanoparticles. *J. Am. Chem. Soc.* **2003**, *125*, 13940–13941.
20. Pernodet, N.; Fang, X.; Sun, Y.; Bakhtina, A.; Ramakrishnan, A.; Sokolov, J.; Ulman, A.; Rafailovich, M. Adverse Effects of Citrate/Gold Nanoparticles on Human Dermal Fibroblasts. *Small* **2006**, *2*, 766–773.
21. Hauck, T. S.; Ghazani, A. A.; Chan, W. C. Assessing the Effect of Surface Chemistry on Gold Nanorod Uptake, Toxicity, and Gene Expression in Mammalian Cells. *Small* **2008**, *4*, 153–159.
22. Khan, J. A.; Pillai, B.; Das, T. K.; Singh, Y.; Maiti, S. Molecular Effects of Uptake of Gold Nanoparticles in HeLa Cells. *Chembiochem.* **2007**, *8*, 1237–1240.
23. Pan, Y.; Neuss, S.; Leifert, A.; Fischler, M.; Wen, F.; Simon, U.; Schmid, G.; Brandau, W.; Jahnen-Dechent, W. Size-Dependent Cytotoxicity of Gold Nanoparticles. *Small* **2007**, *3*, 1941–1949.
24. Park, S.; Lee, Y. K.; Jung, M.; Kim, K. H.; Chung, N.; Ahn, E. K.; Lim, Y.; Lee, K. H. Cellular Toxicity of Various Inhalable Metal Nanoparticles on Human Alveolar Epithelial Cells. *Inhal. Toxicol.* **2007**, *19*, 59–65.
25. Xia, T.; Kovochich, M.; Brant, J.; Hotze, M.; Sempf, J.; Oberley, T.; Sioutas, C.; Yeh, J. I.; Wiesner, M. R.; Nel, A. E. Comparison of the Abilities of Ambient and Manufactured Nanoparticles to Induce Cellular Toxicity According to an Oxidative Stress Paradigm. *Nano Lett.* **2006**, *6*, 1794–1807.
26. Zhang, Z.; Berg, A.; Levanon, H.; Fessenden, R. W.; Meisel, D. On the Interaction of Free Radicals with Gold Nanoparticles. *J. Am. Chem. Soc.* **2003**, *125*, 7959–7963.
27. Derfus, A. M.; Chan, W. C. W.; Bhatia, S. N. Intracellular Delivery of Quantum Dots for Live Cell Labeling and Organelle Tracking. *Adv. Mater.* **2004**, *16*, 961–966.
28. Yang, H.; Liu, C.; Yang, D.; Zhang, H.; Xi, Z. Comparative Study of Cytotoxicity, Oxidative Stress and Genotoxicity Induced by Four Typical Nanomaterials: The Role of Particle Size, Shape and Composition. *J. Appl. Toxicol.* **2008**, DOI 10.1002/jat.1385.
29. Park, E. J.; Yi, J.; Chung, K. H.; Ryu, D. Y.; Choi, J.; Park, K. Oxidative Stress and Apoptosis Induced by Titanium Dioxide Nanoparticles in Cultured BEAS-2B Cells. *Toxicol. Lett.* **2008**, *180*, 222–229.
30. Boonstra, J.; Post, J. A. Molecular Events Associated with Reactive Oxygen Species and Cell Cycle Progression in Mammalian Cells. *Gene* **2004**, *337*, 1–13.
31. Turrens, J. F. Mitochondrial Formation of Reactive Oxygen Species. *J. Physiol.* **2003**, *552*, 335–344.
32. Kumar, C. *Nanomaterials-Toxicity, Health and Environmental Issues*; Wiley- VCH Verlag GmbH & Co: Weinheim, Germany, 2006; Vol. 5.
33. Yang, H. C.; Pon, L. A. Toxicity of Metal Ions Used in Dental Alloys: A Study in the Yeast *Saccharomyces cerevisiae*. *Drug Chem. Toxicol.* **2003**, *26*, 75–85.
34. Schreurs, W. J.; Rosenberg, H. Effect of Silver Ions on Transport and Retention of Phosphate by *Escherichia coli*. *J. Bacteriol.* **1982**, *152*, 7–13.
35. Dibrov, P.; Dzioba, J.; Gosink, K. K.; Hase, C. C. Chemiosmotic Mechanism of Antimicrobial Activity of Ag(+) in *Vibrio cholerae*. *Antimicrob. Agents Chemother.* **2002**, *46*, 2668–2670.
36. Bragg, P. D.; Rainnie, D. J. The Effect of Silver Ions on the Respiratory Chain of *Escherichia coli*. *Can. J. Microbiol.* **1974**, *20*, 883–889.

37. Friedrich, T. The NADH:Ubiquinone Oxidoreductase (Complex I) from *Escherichia coli*. *Biochim. Biophys. Acta* **1998**, *1364*, 134–146.
38. Liau, S. Y.; Read, D. C.; Pugh, W. J.; Furr, J. R.; Russell, A. D. Interaction of Silver Nitrate with Readily Identifiable Groups: Relationship to the Antibacterial Action of Silver Ions. *Lett. Appl. Microbiol.* **1997**, *25*, 279–283.
39. Holt, K. B.; Bard, A. J. Interaction of Silver(I) Ions with the Respiratory Chain of *Escherichia coli*: An Electrochemical and Scanning Electrochemical Microscopy Study of the Antimicrobial Mechanism of Micromolar Ag+. *Biochemistry* **2005**, *44*, 13214–13223.
40. Yamanaka, M.; Hara, K.; Kudo, J. Bactericidal Actions of a Silver Ion Solution on *Escherichia coli*, Studied by Energy-Filtering Transmission Electron Microscopy and Proteomic Analysis. *Appl. Environ. Microbiol.* **2005**, *71*, 7589–7593.
41. Ishikawa, K.; Ishii, H.; Saito, T. DNA Damage-Dependent Cell Cycle Checkpoints and Genomic Stability. *DNA Cell Biol.* **2006**, *25*, 406–411.
42. Fenech, M. Cytokinesis-Block Micronucleus Assay Evolves into a "Cytome" Assay of Chromosomal Instability, Mitotic Dysfunction and Cell Death. *Mutat. Res.* **2006**, *600*, 58–66.
43. Cadet, J.; Delatour, T.; Douki, T.; Gasparutto, D.; Pouget, J. P.; Ravanat, J. L.; Sauvaigo, S. Hydroxyl Radicals and DNA Base Damage. *Mutat. Res.* **1999**, *424*, 9–21.
44. Arakawa, H.; Neault, J. F.; Tajmir-Riahi, H. A. Silver(I) Complexes with DNA and RNA Studied by Fourier Transform Infrared Spectroscopy and Capillary Electrophoresis. *Biophys. J.* **2001**, *81*, 1580–1587.
45. Hossain, Z.; Huq, F. Studies on the Interaction Between Ag(+) and DNA. *J. Inorg. Biochem.* **2002**, *91*, 398–404.
46. Wong, L. Y.; Recht, J.; Laurent, B. C. Chromatin Remodeling and Repair of DNA Double-Strand Breaks. *J. Mol. Histol.* **2006**, *37*, 261–269.
47. Sweet, S.; Singh, G. Accumulation of Human Promyelocytic Leukemic (HL-60) Cells at Two Energetic Cell Cycle Checkpoints. *Cancer Res.* **1995**, *55*, 5164–5167.
48. Mroz, R. M.; Schins, R. P.; Li, H.; Drost, E. M.; Macnee, W.; Donaldson, K. Nanoparticle Carbon Black Driven DNA Damage Induces Growth Arrest and AP-1 and NFkappaB DNA Binding in Lung Epithelial A549 Cell Line. *J. Physiol. Pharmacol.* **2007**, *58*, 461–470.
49. Nativo, P.; Prior, I. A.; Brust, M. Uptake and Intracellular Fate of Surface-Modified Gold Nanoparticles. *ACS Nano* **2008**, *2*, 1639–1644.
50. Zhao, Y.; Nalwa, H. S. *Nanotoxicology—Interactions of Nanomaterials with Biological Systems*; American Scientific: Los Angeles, CA, 2007.
51. Swanson, J. A. Shaping Cups into Phagosomes and Macropinosomes. *Nat. Rev. Mol. Cell Biol.* **2008**, *9*, 639–649.
52. Vallhov, H.; Qin, J.; Johansson, S. M.; Ahlborg, N.; Muhammed, M. A.; Scheynius, A.; Gabrielsson, S. The Importance of an Endotoxin-Free Environment During the Production of Nanoparticles Used in Medical Applications. *Nano Lett.* **2006**, *6*, 1682–1686.
53. http://www.cyto.purdue.edu/flowcyt/software/Winmdi.htm.
54. Rudolf, E.; Cervinka, M. The Role of Intracellular Zinc in Chromium(VI)-Induced Oxidative Stress, DNA Damage and Apoptosis. *Chem. Biol. Interact.* **2006**, *162*, 212–227.
55. Murugavel, P.; Pari, L.; Sitasawad, S. L.; Kumar, S.; Kumar, S. Cadmium Induced Mitochondrial Injury and Apoptosis in Vero Cells: Protective Effect of Diallyl Tetrasufide from Garlic. *Int. J. Biochem. Cell Biol.* **2007**, *39*, 161–170.
56. Poonepalli, A.; Balakrishnan, L.; Khaw, A. K.; Low, G. K.; Jayapal, M.; Bhattacharjee, R. N.; Akira, S.; Balajee, A. S.; Hande, M. P. Lack of Poly(ADP-ribose) Polymerase-1 Gene Product Enhances Cellular Sensitivity to Arsenite. *Cancer Res.* **2005**, *65*, 10977–10983.
57. Hande, M. P.; Boei, J. J.; Natarajan, A. T. Induction and Persistence of Cytogenetic Damage in Mouse Splenocytes Following Whole-Body X-Irradiation Analysed by Fluorescence *In Situ* Hybridization. II. Micronuclei. *Int. J. Radiat. Biol.* **1996**, *70*, 375–383.
58. Oliveira, R. J.; Matuo, R.; da Silva, A. F.; Matiazi, H. J.; Mantovani, M. S.; Ribeiro, L. R. Protective Effect of Beta-Glucan Extracted from *Saccharomyces cerevisiae*, Against DNA Damage and Cytotoxicity in Wild-Type (k1) and Repair-Deficient (xrs5) CHO Cells. *Toxicol. In Vitro* **2007**, *21*, 41–52.